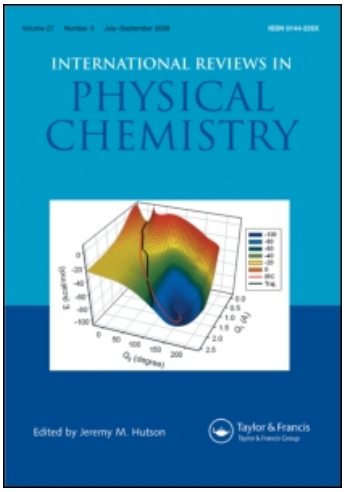

International Reviews in Physical Chemistry
Publication details, including instructions for authors and subscription information:
http://www.informaworld.com/smpp/title~content=t713724383

Recent advances in understanding the structures of medium-sized protonated water clusters

Huan-Cheng Chang[a]; Chih-Che Wu[a]; Jer-Lai Kuo[b]
[a] Institute of Atomic and Molecular Sciences, Academia Sinica, Taipei, Taiwan 106, R.O.C [b] School of Physical and Mathematical Sciences, Nanyang Technological University, 1 Nanyang Walk, Singapore 637616, Singapore

To cite this Article Chang, Huan-Cheng , Wu, Chih-Che and Kuo, Jer-Lai(2005) 'Recent advances in understanding the structures of medium-sized protonated water clusters', International Reviews in Physical Chemistry, 24: 3, 553 — 578
To link to this Article: DOI: 10.1080/01442350500448116
URL: http://dx.doi.org/10.1080/01442350500448116

International Reviews in Physical Chemistry,
Vol. 24, Nos. 3–4, July–December 2005, 553–578

Taylor & Francis
Taylor & Francis Group

Recent advances in understanding the structures of medium-sized protonated water clusters

HUAN-CHENG CHANG*†, CHIH-CHE WU† and JER-LAI KUO‡

†Institute of Atomic and Molecular Sciences, Academia Sinica,
PO Box 23-166, Taipei, Taiwan 106, R.O.C
‡School of Physical and Mathematical Sciences, Nanyang Technological University,
1 Nanyang Walk, Singapore 637616, Singapore

(*Received 9 October 2005*)

Understanding the structures of medium-sized protonated water clusters $[H^+(H_2O)_n]$ has made a significant advancement recently thanks to the development of new experimental techniques and high-level computational methods. A combination of vibrational predissociation spectroscopy and *ab initio* calculations was shown to be effective in elucidating the structures of the clusters as a function of their temperature and size. The combined study revealed several intriguing features (such as symmetric hydrogen bonds) that could not be found for neutral water clusters. However, similar to its neutral counterpart, the number of stable isomers increases exponentially with cluster size (n), making direct structural identification of medium-sized clusters difficult. Despite the difficulties, both experimental and computational results indicated a smooth change in hydrogen-bond topology from tree-like, single-ring, multiple-ring to polyhedron-like structures (and their mixtures) as n increases from 5 to 28. The excess proton can be symmetrically hydrated at $n = 6$–8. Five-membered ring isomers can form at $n = 7$ and 8 as the low-lying minima. Only a single feature ($\sim$3695 cm^{-1}) in the free OH stretching region was observed for $H^+(H_2O)_{21}$ and $H^+(H_2O)_{28}$, suggesting that all surface water molecules are linked in a similar 3-coordinated (double-acceptor-single-donor, (AAD)) configuration in both "magic number" clusters. The clathrate-like structures open up at higher temperatures, as evidenced by the increased intensity of the free-OH stretching absorption band ($\sim$3715 cm^{-1}) of 2-coordinated (single-acceptor-single-donor, (AD)) water molecules. Further understanding of the structures and thermal properties of these clusters is gained through the studies with Monte Carlo (MC) and molecular dynamics simulations, ion reactivity and thermal dissociation measurements, as well as Ar tagging experiments.

Contents

*Corresponding author. Email: hcchang@po.iams.sinica.edu.tw

International Reviews in Physical Chemistry
ISSN 0144–235X print/ISSN 1366–591X online
http://www.tandf.co.uk/journals
DOI: 10.1080/01442350500448116

1. Introduction

Studies of clusters bridge the gap of our understanding of isolated molecules and bulk phases. Much of the progress in this direction has been achieved for neutral water clusters [1–5]. In contrast, charged water clusters have been less characterized and understood. These clusters (either protonated or deprotonated) are common in nature and play important roles in many fields of science including atmospheric chemistry, solution chemistry, and biological chemistry. Protonated water clusters, in particular, are the most abundant cluster ions in the stratosphere and they participate actively in a variety of atmospheric nucleation and reactions associated with water [6, 7]. It is known [8] that the presence of excess protons has a profound influence on the phase transition of small water aggregates under atmospheric conditions. However, up to date, the critical size beyond which protonated water clusters resemble bulk water remains undetermined. Although changing the size of the clusters in principle allows one to study systematically and comprehensively the transition of hydrated protons (or hydrated hydroxide ions) from isolated molecules to the bulk, some subtleties on the structure and dynamics arising from the complex hydrogen bonding networks have projected this problem challenging and interesting.

Because of its importance in the atmosphere and also in the biosphere, protonated water cluster $H^+(H_2O)_n$ has been one of the most extensively investigated gas-phase cluster ions in the laboratory as well as in the field. While small-sized clusters (say $n \leq 4$) have been studied in detail both experimentally [9–14] and theoretically [15–18], considerably less is known for cluster ions of medium sizes. This is partially because when the cluster size increases, the number of possible structural configurations increase exponentially, making it very difficult to distinguish the global minima from various topologically different but energetically similar isomers. Challenges are also encountered on the experimental side, where the observed infrared spectra are always broad and nearly featureless (particularly in the hydrogen-bonded OH stretching region) due to the difficulty of producing vibrationally cold species and the coexistence of many energetically similar isomers.

Recently, high-resolution mass spectrometry, infrared spectroscopy, high-level *ab initio* calculations, Monte Carlo (MC), and molecular dynamics simulations have been applied together to deduce the information about the structures and thermal properties of protonated water clusters over a wide size range. The studies can be roughly separated into three groups according to the size of the clusters examined: small, medium, and large. It is not the aim of this article to review the status of our current

understanding of small-sized clusters, since they have been closely examined in 1989 by Yeh *et al*. [10] for the OH stretching modes of $H^+(H_2O)_{2-4}$ at 2800–3800 cm^{-1} and more recently by Asmis *et al*. [12] and Fridgen *et al*. [13, 14] for the proton vibrational modes of $H^+(H_2O)_2$ at 600–2000 cm^{-1}. Moreover, many theoretical works that treat all degrees of freedom to attain the detailed structures of $H_5O_2^+$ have been reported, and they have been properly reviewed in some recent articles [16–18]. The main task of this review is to summarize the recent advances in exploring the complex potential energy surfaces of medium-sized clusters (say $n \leq 30$), which are now amendable to both experimental and theoretical investigations. An article covering larger $H^+(H_2O)_n$ clusters (say $n > 30$) studied with Fourier-transform ion cyclotron resonance mass spectrometry has been provided by Niedner-Schatteburg and Bondybey [19].

With respect to the theoretical treatment of $H^+(H_2O)_n$, the review article of Kochanski *et al*. [15] has conveyed most (if not all) of the information before 1997. However, a large number of theoretical papers appeared in the literature since then, which makes a thorough review impractical. Furthermore, there is a considerable amount of studies on the investigation of proton transfer in liquid and solid phases. In order to keep this review in a reasonable length, we focus mainly on the recent (that is, after 1997) investigations of medium-sized protonated water clusters (i.e. $H^+(H_2O)_{5-30}$), and earlier works included only when needed. Due to the short period of time covered, we do not attempt to give a historical account as Kochanski *et al*. [15] but instead a concise review will be given. In this article, after a brief discussion of the techniques used for the studies in both experiment and theory sections, some salient features of the experimental and computational findings are discussed.

2. Experiments

Experimental studies of medium-sized protonated water clusters can be traced back to 1967. Kebarle and coworkers [20–22] conducted one of the first thermochemical measurements for binding energies of size-selected $H^+(H_2O)_n$ in the gas phase. Ensuing investigations encompassed unimolecular dissociations [23–25] and ion–molecule reactions [26–28] of importance in the stratosphere [29, 30], in aqueous solution [31] as well as in biological systems [32, 33]. Recently, gas-phase reactions of $H^+(H_2O)_n$ with various small molecules were re-examined for their size-dependent reaction cross sections [27, 28]. However, to understand the nature of the thermochemistry as well as the corresponding size-dependent reactivity, knowledge of the structure of each cluster is required. Vibrational predissociation spectroscopy, as pioneered by Lee and coworkers [9–11], has emerged as one of the most powerful and direct probes for the hydrogen-bonding network of $H^+(H_2O)_n$. The method has been actively applied by a number of groups since 1989 [34–43] to elucidate the structure of medium-sized water clusters ($n = 5$–30). While most of the works are focused on the fundamental OH stretching vibrations, extension of the study to the first overtone region has been attempted by Wu *et al*. [38].

The experimental setup used to obtain vibrational predissociation spectra of $H^+(H_2O)_n$ typically consists of an ion source, a tandem mass spectrometer, and an infrared laser system (figure 1). The design of the ion source determines the temperature

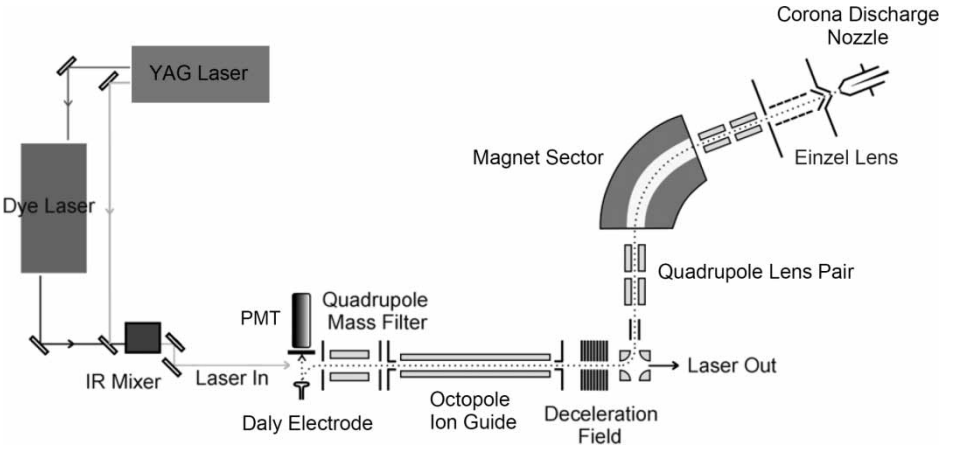

Figure 1. Schematic diagram of a vibrational predissociation tandem mass spectrometer and a pulsed infrared laser system [48].

and, therefore, the structure of the clusters produced. The source can be a continuous corona-discharged molecular beam [37], an electron-beam-ionized supersonic expansion [42, 43], or a laser plasma molecular beam [43]. The tandem mass spectrometer can consist of a magnet sector and a quadrupole [37], two quadrupoles in series [42], or a time-of-flight tube with a mass gate [43]. The tunable infrared photons can be generated from difference frequency mixing of two pulsed lasers [37], an optical parametric oscillator (OPO) laser [43], or a free electron laser [12–14]. At present, most of the experiments were carried out in the mid-infrared region for the OH stretching vibrations. The reason is primarily because the energy required to induce the dissociation, $H^+(H_2O)_n \rightarrow H^+(H_2O)_{n-1} + H_2O$, at $n < 30$ is in the range of $10\,\text{kcal}\,\text{mol}^{-1}$ [44], which is comparable to the energy of the infrared photons used in the 3 μm region through one-photon absorption process. In the case that the input photon energy is lower than that required for the dissociation, the vibrationally induced reaction can still occur at the expense of some internal energies. Infrared action spectra are then obtained by recording the dissociation fraction as a function of the excitation laser wavelength with the detector operating in an ion counting mode. The principle and practice of the vibrational predissociation technique have been described in depth previously in three review articles in this journal [45–47].

2.1. *Hydrogen-bond topologies*

Figure 2 displays the vibrational predissociation spectra of $H^+(H_2O)_n$, $n = 5$–7 and 9–11, acquired with the experimental setup shown in figure 1 [48]. The clusters were generated from a continuous corona-discharged supersonic expansion of H_2O seeded in pure H_2 at a backing pressure of ~200 Torr. Two types of spectral features can be distinguished according to the hydrogen-bonding status of the OH bonds: the free-OH stretches at 3600–3800 cm^{-1} and the hydrogen-bonded OH stretches at 2800–3600 cm^{-1}. As seen, the spectrum gradually loses distinct spectral signatures in the bonded-OH stretching region as the cluster size increases to $n = 9$, presumably, because of the coexistence of several structural isomers in the supersonic expansion.

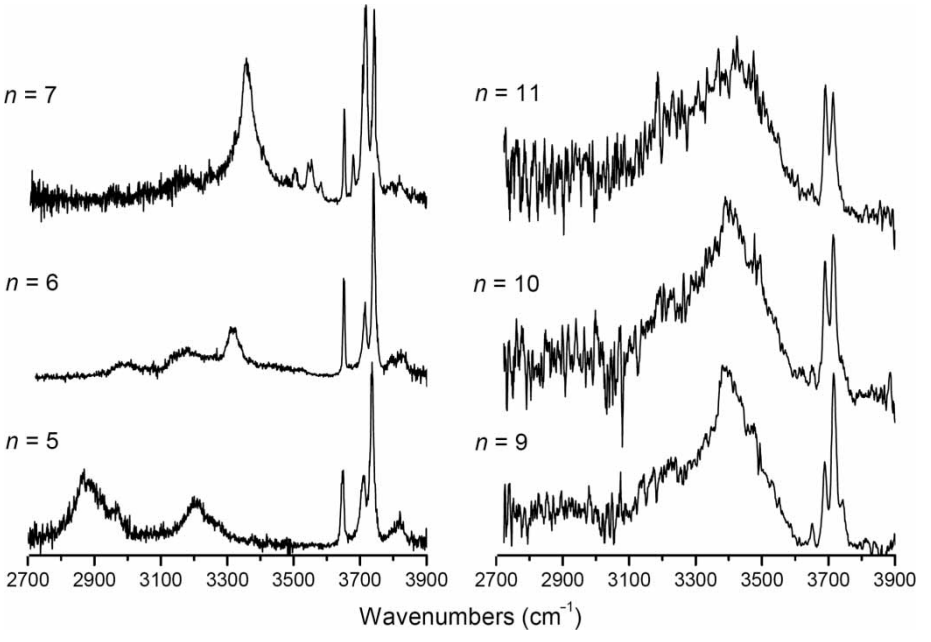

Figure 2. Vibrational predissociation spectra of $H^+(H_2O)_n$, $n = 5$–7 and 9–11, in the frequency range of 2700–3900 cm^{-1} [37, 41].

For the free-OH stretches, they can be further separated into three groups: (1) symmetric and asymmetric stretches (~3650 and ~3740 cm^{-1}) of 1-coordinated H_2O acting as a single-acceptor (A), (2) free-OH stretches (~3715 cm^{-1}) of 2-coordinated H_2O acting as a single-acceptor-single-donor (AD), and (3) free-OH stretches (~3690 cm^{-1}) of 3-coordinated H_2O acting as a double-acceptor-single-donor (AAD). Notably, these four free-OH stretches are distinct in frequency, and the corresponding absorption bands are sharp (~10 cm^{-1}) and well-solved, proving rich structural information. In comparison, the absorption bands in the bonded-OH stretching region are congested, broad (~100 cm^{-1}), and essentially featureless at $n \geq 9$. A noticeable exception is that relatively sharp features emerge between 3500 and 3600 cm^{-1} at the cluster size $n = 7$ (figure 2). In particular, the doublet appearing at 3544 and 3555 cm^{-1} matches well in frequency with the spectral signatures of a symmetric four-membered ring structure of $NH_4^+(H_2O)_5$ [48], and they correspond to the bonded-OH stretches of two AD water molecules involved in a five-membered ring formation [37]. The other two sharp peaks at 3502 and 3581 cm^{-1} can be assigned to a second five-membered ring isomer but with an asymmetric structure [37].

Intriguing spectral evolution is seen for the free-OH stretches of $H^+(H_2O)_n$ starting from $n = 4$ to $n = 25$ (figure 3). As the cluster size increases, the symmetric and asymmetric stretching bands (~3650 and ~3740 cm^{-1}) of the free-OH groups of 1-coordinated H_2O diminish in intensity, and they vanish nearly completely at $n = 11$. In contrast, the free-OH stretching band (3715 cm^{-1}) of 2-coordinated H_2O first appears at $n = 5$, increases in intensity at $n = 6$–8, becomes dominant at $n = 9$, but soon loses its dominance at $n = 11$. Finally, the band (3690 cm^{-1}) associated with the free-OH

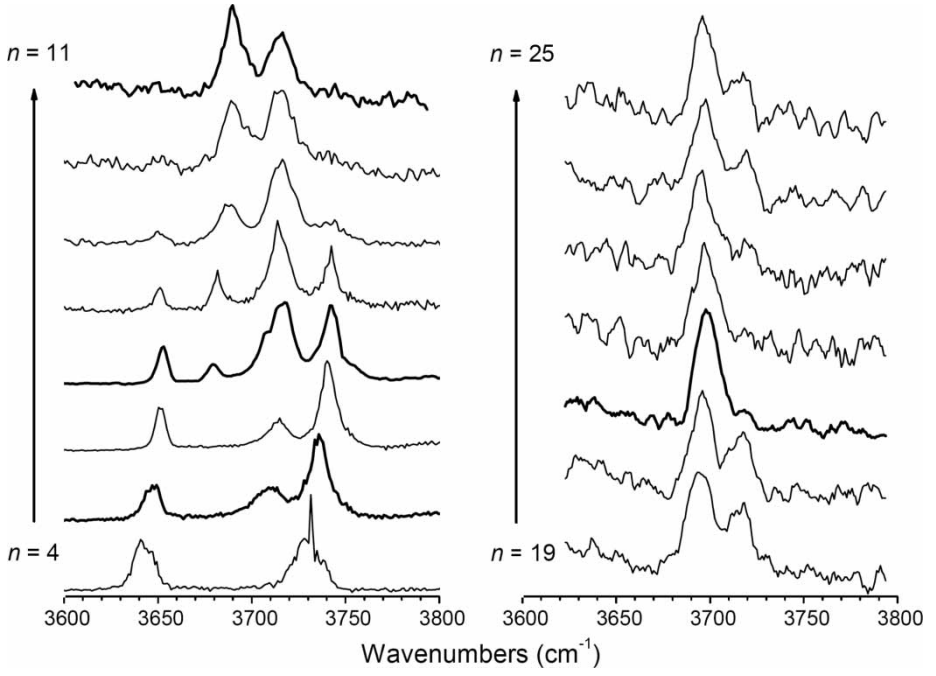

Figure 3. Vibrational predissociation spectra of $H^+(H_2O)_{4-11}$ and $H^+(H_2O)_{19-25}$ in the free-OH stretching region [37, 40, 41].

stretches of 3-coordinated H_2O emerges at $n=7$ and becomes dominant in the spectra of $n=11$ and even larger clusters [41]. Such size-dependent spectral changes (and thus the structural changes of the clusters) are general and have been similarly observed by Miyazaki *et al.* [42] and Shin *et al.* [43] using different ion sources to produce the same $H^+(H_2O)_n$ clusters.

Three distinct structural transition points can be identified in the infrared action spectra. The first transition appears at $n=5$ when the second solvation shell of the H_3O^+ ion core forms, as revealed by the emergence of the free-OH stretching band of 2-coordinated H_2O at $\sim 3710\,cm^{-1}$. The second transition occurs at $n=7$ when the ring isomers take shape, as evidenced by the observation of the free-OH stretching band 3-coordinated H_2O at $\sim 3690\,cm^{-1}$ as well as the emergence of the bonded-OH stretches between 3500 and $3600\,cm^{-1}$ (figure 2). The third transition is highlighted by the takeover of the predominance of the spectra by the 3-coordinated H_2O at $n=11$, where multiple-ring and/or cage-like isomers prevail. Following the trend of this transition, one may expect the absorption band centering around $3690\,cm^{-1}$ to dominate as n further increases. Indeed, the $3690\,cm^{-1}$ band is the only feature observed in the free-OH stretching region for the $n=21$ and 22 clusters (figure 3). This unique feature has been confirmed independently by four different research groups [37, 42, 43] with use of the same vibrational predissociation techniques for $H^+(H_2O)_n$ up to $n=28$. It should be noted that the same absorption band at $\sim 3690\,cm^{-1}$ has been previously identified as the dangling OH stretch of 3-coordinated water molecules on the surfaces

of thermally annealed nanometer-sized ice clusters [5, 49–51]. It is also the fingerprint for identification of the pentagonal clathrate structure of "magic number" water clusters.

2.2. *"Magic number" clusters*

One of the long-standing interests of $H^+(H_2O)_n$ concerns the structure of the magic number cluster $H^+(H_2O)_{21}$ [23–25, 52–60]. The cluster ion was first identified in 1973 by Lin [52], who observed an intensity anomaly in the mass spectrum at m/z 379 corresponding to 21 water molecules with an excess proton. Subsequent ion reactivity measurements [55–60] showed that the $n=22$ cluster decays significantly faster than its adjacent ions. Searcy and Fenn [53] attributed the observed anomalies to the formation of an exceptionally stable isomer of $H^+(H_2O)_{21}$. The isomer has a structure analogous to that of its neutral hydrate Ar-$(H_2O)_{20}$ [61], which is composed of a pentagonal (5^{12}). Suggestion of this clathrate-like structure with a hydronium ion in the cage center is favored in this and other early mass spectrometric studies of $H^+(H_2O)_{21}$ [58].

Vibrational signatures of the magic number cluster $H^+(H_2O)_{21}$ were identified very recently by Miyazaki *et al.* [42] and Shin *et al.* [43] for the OH stretching vibrations of $H^+(H_2O)_n$ produced from three different ion sources. Shin *et al.* found that even though the intensity profile of the mass spectrum did not show a pronounced anomaly at $n=21$, the infrared spectra of $H^+(H_2O)_n$ in the free-OH stretching region displayed only a single band at $\sim$3695 cm^{-1} of the $n=21$ and 22 clusters but a doublet at $\sim$3695 and $\sim$3715 cm^{-1} for the neighboring ions. The spectral simplification at $n=21$ is a strong indication that all dangling OH groups in the cluster arise from water molecules in similar binding sites, a result consistent with the aforementioned 5^{12} clathrate structure enclosing either one H_2O molecule or an H_3O^+ ion in the cage. Similar observations were made by Miyazaki *et al.* in a warmer molecular beam, although the authors observed two absorption bands in the same frequency range, indicating the coexistence of 5^{12} and non-5^{12} structural isomers. Unfortunately, as discussed in the earlier section, no distinct spectral signatures could be observed in the hydrogen-bonded OH stretching region to assist further structural identification of this cluster isomer.

In view of the complexity of the system and the likelihood that the structure of $H^+(H_2O)_{21}$ investigated experimentally cannot be confirmed by a single piece of evidence, Wu *et al.* [40] took a different approach to deal with this problem. The approach involved simultaneous measurements for the mass spectra, dissociation fractions, and infrared spectra of $H^+(H_2O)_n$ produced in the vicinity of $n=21$ using the same ion source but under different supersonic expansion conditions. Figure 4 summarizes the results of these experiments. Indeed, with use of a higher backing pressure behind a corona-discharge nozzle to produce colder clusters (figure 4a and 4b), three anomalies were observed simultaneously, including (1) the peak at $n=21$ is more intense than its neighboring ions in the mass spectrum, (2) the size-dependent dissociation fractions show a distinct drop for the 21-mer, and (3) the infrared spectrum of $H^+(H_2O)_{21}$ exhibits only a single feature at 3699 cm^{-1}, corresponding to the free-OH stretching of 3-coordinated water molecules. The spectroscopic observations, consistent with that of Shin *et al.* [43], suggest the formation of a 5^{12} clathrate structure. The dodecahedral cage "melts" at higher temperatures (figure 4c), as evidenced by the

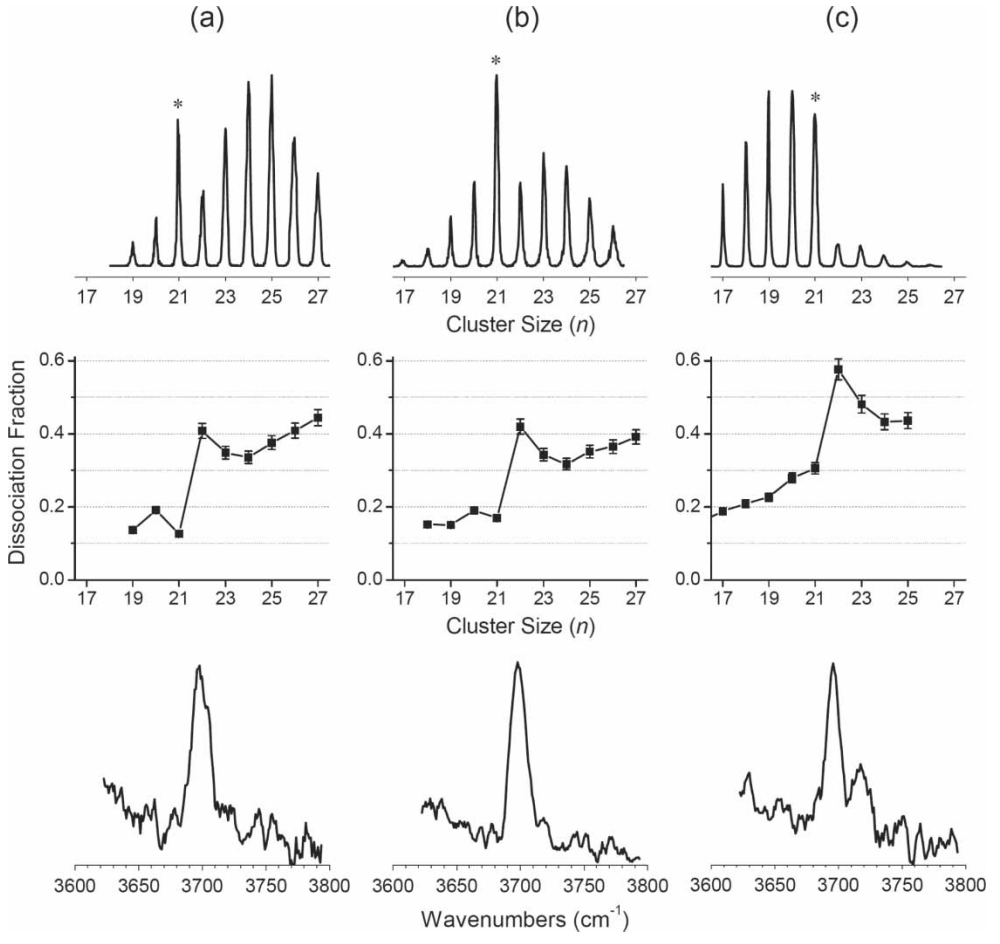

Figure 4. Comparison of mass spectra, dissociation fractions, and vibrational predissociation spectra of $H^+(H_2O)_{21}$ clusters produced under three different supersonic expansion conditions: (a) backing pressure of 340 Torr; gas composition of 1% Ar and saturated H_2O vapor in H_2, (b) backing pressure of 200 Torr; gas composition of saturated H_2O vapor in H_2, (c) backing pressure of 120 Torr; gas composition of saturated H_2O vapor in H_2. The $H^+(H_2O)_{21}$ peaks are denoted by asterisks (*) [40].

emergence of a free-OH stretching feature at 3717 cm^{-1} for the 2-coordinated water molecules of $H^+(H_2O)_{21}$ produced in a warmer beam, in accord with the observation of Miyazaki *et al.* [42].

Wu *et al.* [40] have applied further this combined technique to the study of $H^+(H_2O)_{28}$, which is the second smallest water cluster that exhibits an intensity enhancement in the mass spectrum [62, 63]. This intensity enhancement, however, is not always seen depending on the beam expansion condition. Figure 5a shows the mass spectrum of the protonated water clusters produced by a corona-discharged supersonic expansion (cf. figure 1) at a backing pressure of 340 Torr near $n = 28$, where the intensity anomaly can be clearly detected. As in the case of $H^+(H_2O)_{21}$, the dissociation fraction displays a distinct drop at $n = 28$ and good correlation is established between

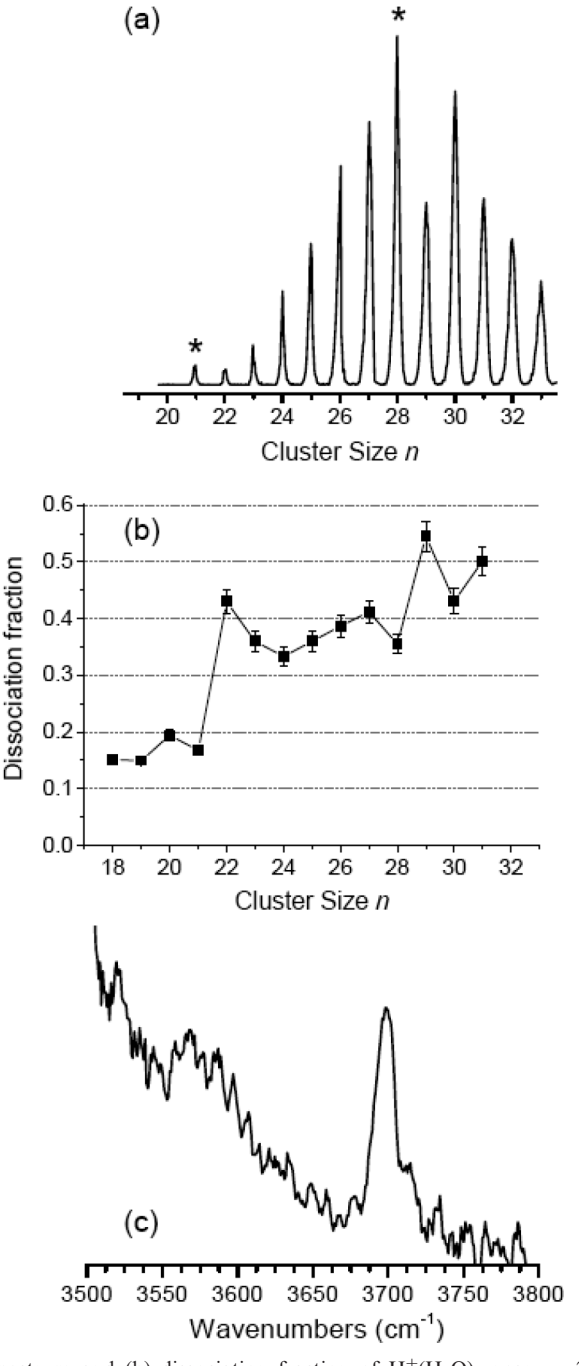

Figure 5. (a) Mass spectrum and (b) dissociation fraction of $H^+(H_2O)_n$ near $n = 28$. The clusters were produced at a backing pressure of 340 Torr; gas composition of 1% Ar and saturated H_2O vapor in H_2. The $n = 21$ and $n = 28$ peaks are denoted by asterisks (*). (c) Vibrational predissociation spectrum of $H^+(H_2O)_{28}$ in the free-OH stretching region [40].

the ion intensity and the dissociation fraction measurements (figure 5b). Again, predominantly only a single free-OH stretching feature is detected at 3698 cm^{-1} in the vibrational predissociation spectrum of $H^+(H_2O)_{28}$ under cold supersonic expansion conditions (figure 5c). The spectroscopic observation is consistent with the suggestion that this magic number cluster ion is composed of a pentakaidecahedral ($5^{12}6^3$ or $5^66^35^6$) cage enclosing two water molecules in the form of either H_3O^+–H_2O or H_2O–H_2O [40, 63].

2.3. *Symmetric proton hydration*

A feature of particular interest in $H^+(H_2O)_n$ is the symmetric hydrogen bond. It has been long speculated that the cluster ion can exist either as an H_3O^+-centered $[H_3O^+(H_2O)_{n-1}]$ or an $H_5O_2^+$-centered $[H_5O_2^+(H_2O)_{n-2}]$ isomer with the extra proton being bound to one or two water molecules, respectively. Which of the above possibilities prevails depends sensitively on the structure and solvation number of the clusters. From early experimental investigations of bulk water, a structure with a closed first solvation shell around an H_3O^+ cation was inferred, $H_3O^+(H_2O)_3$ (known as the Eigen cation) [64, 65]. Infrared spectra of aqueous acidic solutions, however, were interpreted in terms of a protonated water dimer, $H_5O_2^+$ (known as the Zundel cation) [66, 67]. For the gas-phase clusters, infrared spectroscopic measurements by Yeh *et al.* [10] determined that the predominant form of $H^+(H_2O)_4$ is $H_3O^+(H_2O)_3$. No spectral evidence was found for the existence of the linear $H_5O_2^+(H_2O)_2$ structure, which is a stable isomer with the excess proton equally shared by two water dimers [37]. The failure to identify this isomer can be easily rationalized by considering that the hydration shell of the Zundel-like cation is incomplete at $n=4$ and hence it is significantly less stable than the corresponding Eigen cation.

The Zundel cation $H_5O_2^+$, on the other hand, can be fully hydrated at $n=6$. The formation of $H_5O_2^+(H_2O)_4$ is energetically favorable, making possible identification of this intriguing structure containing a symmetric hydrogen bond around the excess proton (figure 6). This structural identification, however, is non-trivial because most of the $H^+(H_2O)_6$ isomers are asymmetric with the Eigen-type structure. Furthermore, compared to the cases of $H^+(H_2O)_2$ and $H^+(H_2O)_4$, there exist many more energetically similar forms near the global minima on the potential energy surfaces at $n=6$. Such difficulties are already shown in the early work of Yeh *et al.* [10] who found that the isolated $H_5O_2^+$ cation is Zundel-like with a C_2 symmetry, but it abruptly loses its symmetry (with $H_5O_2^+$ itself becoming C_s symmetry) upon attachment of a weakly interacting ligand such as H_2. This abrupt change in cluster structure was similarly observed in recent Ar tagging experiments [68–70], where the study of $H_5O_2^+$-Ar_n has been extended to the 10 μm region to probe directly the vibrations of the hydrated proton with a high-power OPO laser.

Experimental identification of $H_5O_2^+(H_2O)_4$ is somewhat indirect because of the presence of more than one isomers in the size-selected $H^+(H_2O)_6$ beam. Despite of the complexity, Jiang *et al.* [37] managed to identify this unique isomer based on the observations that (1) no ring formation occurs at $n \leq 7$ (cf. figure 2) and (2) all neutral H_2O molecules in $H_5O_2^+(H_2O)_4$ are in the form of 1-coordinated configuration. The former observation is the key to the success of this identification because it allows

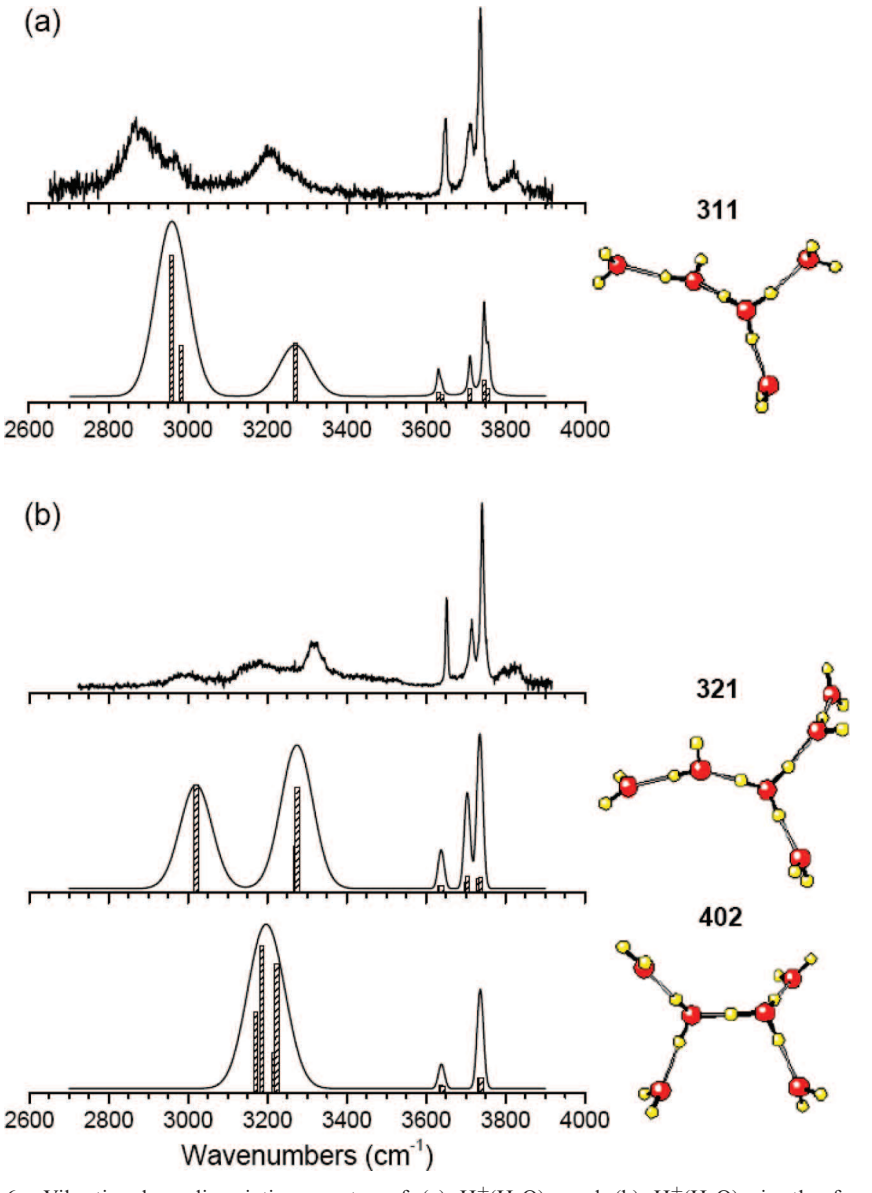

Figure 6. Vibrational predissociation spectra of (a) $H^+(H_2O)_5$ and (b) $H^+(H_2O)_6$ in the free- and bonded-OH stretching region. Structures of two lowest-energy isomers are shown next to the spectra. The O and H atoms are denoted by darker (red) solid spheres and lighter (yellow) open spheres, respectively. The vibrational frequencies of each isomer were computed at the B3LYP/6-31 + G* level with a scaling factor of 0.973. In these three simulated spectra, a bandwidth of 15 cm^{-1} is given for all free-OH stretches and 80 cm^{-1} for all bonded-OH stretches. The reason that the observed intensity ratios between the bonded-OH stretches versus the free-OH stretches are much weaker than the calculated ones is because lower photon energies were used when exciting the bonded-OH stretches [37].

the authors to exclude the possibility of ring isomer formation and therefore simplify the spectral assignment. Figure 6a and 6b display the OH stretching spectra of $H^+(H_2O)_5$ and $H^+(H_2O)_6$, respectively. The observed spectral pattern of $H^+(H_2O)_6$ is in general similar to that of $H^+(H_2O)_5$ with the exception that (1) the free-OH stretching feature at $3710\,cm^{-1}$ decreases in intensity as n increases from 5 to 6, and (2) an additional bonded-OH stretching absorption appears at $3178\,cm^{-1}$ for the $n=6$ cluster. Further comparison of the observed spectra with the *ab initio* calculated spectra (see the next section) in both free- and hydrogen-bonded-OH stretching regions shows a close agreement at $n=5$ for one tree-like H_3O^+-centered isomer. However, satisfactory agreement cannot be reached unless both tree-like H_3O^+-centered and $H_5O_2^+$-centered isomers are taken into consideration (figure 6b). This systematic comparison between observations and calculations provides compelling evidence for the existence of the $H_5O_2^+(H_2O)_4$ isomer in the supersonic expansion.

Similar to $H_5O_2^+(H_2O)_4$, $H_5O_2^+(H_2O)_{5,6}$ can also exist as the lowest-energy isomers of $H^+(H_2O)_{7,8}$, respectively, because of complete solvation of the Zundel-like cation. Identification of the symmetric proton hydration in these bare water clusters has been reported by Jiang *et al.* [37] and, more recently, by Headrick *et al.* [70] with Ar attachment to $H^+(H_2O)_{6-8}$. Efforts to identify the symmetric hydrogen bonds in other cluster systems have also been made by Chang *et al.* [71, 72] for protonated methanol clusters and by Solca and Dopfer [73, 74] for protonated ethanol clusters.

2.4. *Cluster temperatures*

An important parameter to determine in studying the structures of protonated water clusters is the cluster temperature. Nearly all vibrational predissociation spectra reported so far [34–43] were obtained for $H^+(H_2O)_n$ at finite temperatures, at which entropic effects play a significant role in free energy ordering among different isomers. Such temperature information, however, is difficult to deduce for medium-sized clusters because no rotationally resolved features can be observed. Furthermore, no conventional thermometers enable the temperature measurement for clusters produced in a supersonic expansion. Measurement of thermal (or spontaneous) dissociation rates of the clusters in an ion trap offers an attractive alternative for the temperature estimation. Schindler *et al.* [25] made an early attempt along this line for $H^+(H_2O)_{5-65}$ produced from a corona-discharged supersonic expansion and confined in an ion cyclotron resonance (ICR) cell. By measuring the rate of the dissociation induced by black-body infrared radiation and comparing it to the temperature-dependent evaporation rate of ice, they concluded that the most probable temperature of the $H^+(H_2O)_n$ clusters produced in their beam is in the range of 130–140 K.

An approach similar to that of Schindler *et al.* [25] has been applied to estimate the temperature of $H^+(H_2O)_{4-10}$ produced from the corona-discharged ion source shown in figure 1 [40, 41]. The spectrometer described therein contains an octopole ion guide that can be converted to an ion trap by applying two independently controlled pulsed voltages to the two gate electrodes on both ends of the octopole rods. This conversion allowed Lin *et al.* [41] to determine the dissociation fractions of the cluster ions as a function of trapping time, from which the associated cluster

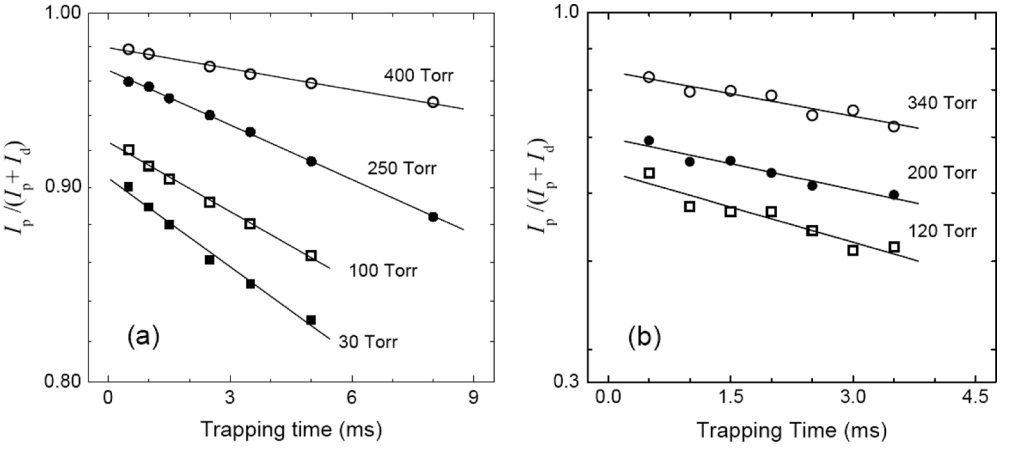

Figure 7. Measurements of dissociation rates for (a) $H^+(H_2O)_9$ and (b) $H^+(H_2O)_{21}$ produced from a corona-discharged molecular beam with various backing pressures behind a room-temperature nozzle. The measurements were conducted in an octopole ion trap and intensities of the parent and daughter cluster ions are denoted by I_p and I_d, respectively. The fitted dissociation rate constants are $k = 2.8 \pm 0.2\,s^{-1}$ (○), $7.3 \pm 0.2\,s^{-1}$ (●), $9.3 \pm 0.5\,s^{-1}$ (□), 11.9 ± 0.9 (■) in (a), and $k = 38 \pm 7\,s^{-1}$ (○), $56 \pm 7\,s^{-1}$, (●) $77 \pm 11\,s^{-1}$ (□) in (b) [40, 41].

temperatures were deduced. Figure 7a shows a typical result for the spontaneous dissociation rate measurement for $H^+(H_2O)_9$ with this vibrational predissociation spectrometer under collision-free conditions. A linear fit to the logarithm of the dissociation fraction versus the trapping time yields the dissociation rate constant. The reason that the dissociation fraction is smaller than 1 at the zero trapping time is because a significant fraction of the clusters break apart (presumably by collision with background gas) during the time of flight from the sector magnet through an electrostatic quadrupole bender and a set of decelerator plates before entering the octopole ion trap (figure 1). Given in the legend of figure 7 are the results of the measurements for $H^+(H_2O)_9$ and $H^+(H_2O)_{21}$. As seen, the spontaneous dissociation rate constant of $H^+(H_2O)_9$ decreases by a factor of 4 as a result of the 15-fold backing pressure increase. Similar observations were made for $H^+(H_2O)_{10}$ and $H^+(H_2O)_{11}$, although the magnitude of the change in the rate constant decreases slightly over the same pressure range.

To deduce cluster temperatures from the spontaneous dissociation rate constants, knowledge of the corresponding dissociation energies is required. Wang *et al.* [39] have determined independently the dissociation energies of $H^+(H_2O)_{4-10}$ with a temperature-variable 22-pole ion trap tandem mass spectrometer (figure 8a). Using low-pressure He or H_2 as buffer gas for collisional thermalization, refrigeration of the ion trap permitted a good control of the temperature of the clusters over the range 77–350 K. Shown in figure 8b is an example for the exponential decay of $H^+(H_2O)_5$ in He buffer gas at 8 different trapping temperatures in the range 190–240 K. Exponential fits to these curves give the rate constants at various temperatures, from which the dissociation energy was obtained from the Arrhenius relation, $k = A\exp(-E_a/k_BT)$ [75]. For $H^+(H_2O)_5$, the dissociation activation energy was determined to be $E_a = 6.8\,kcal\,mol^{-1}$ and it decreases monotonically to $4.0\,kcal\,mol^{-1}$ for $H^+(H_2O)_{10}$ at the cluster

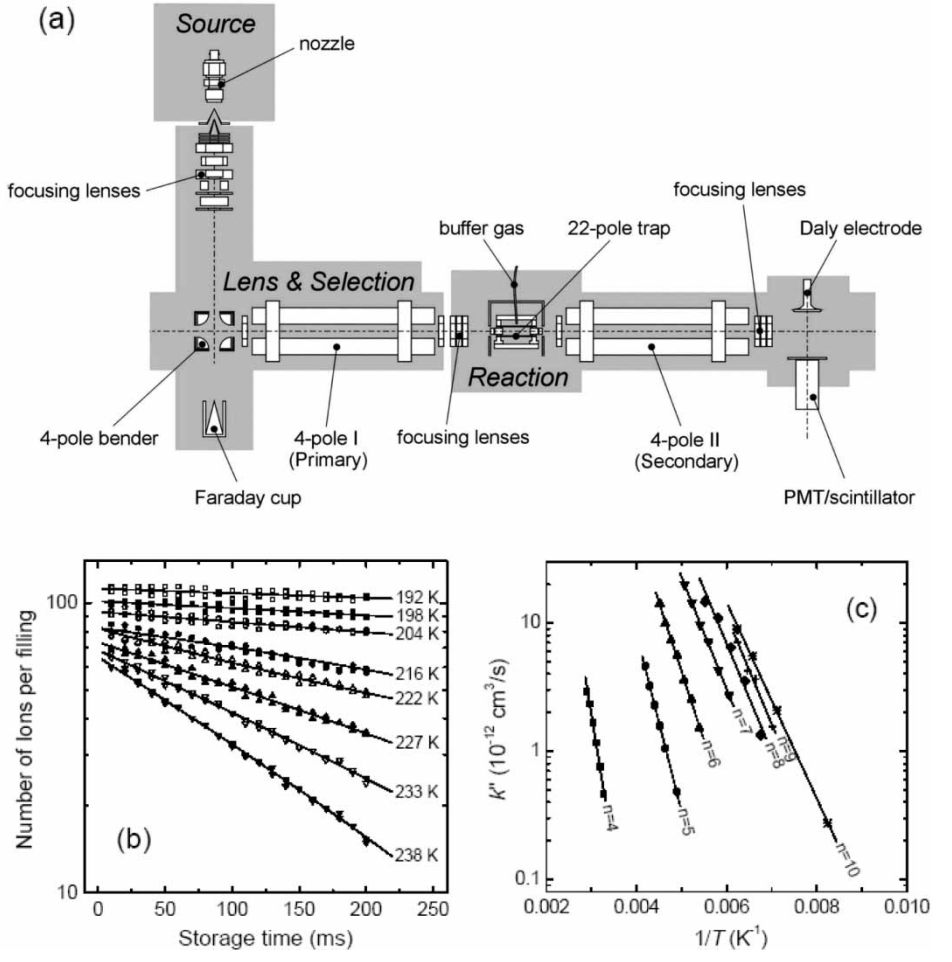

Figure 8. (a) Experimental layout of a 22-pole ion trap tandem mass spectrometer. (b) Dissociation of $H^+(H_2O)_5$ in the temperature-variable 22-pole ion trap at temperatures 192–238 K. (c) Dissociation rate constants of $H^+(H_2O)_{4-10}$ as a function of ion trap temperature. The linear lines represent the best fits of the experimental data to the Arrhenius equation [39].

temperature of ~150 K (figure 8c). Using this energy and the approximation that $A \approx 10^6\,s^{-1}$ [76], Lin *et al.* [41] estimated that the temperature of the $H^+(H_2O)_{9-11}$ clusters produced from their molecular beam for infrared spectroscopic measurements (figure 1) lies in the range of 140–160 K. This temperature is far from 0 K, indicating the thermal effect should be seriously taken into account when identifying the global minima in the potential energy surfaces.

Further refinement of the temperature estimation is possible if precise measurement for the pre-exponential factor A used above in the Arrhenius equation is undertaken. This is achievable with a temperature-variable ICR cell, as demonstrated by Williams and coworkers [76] in the study of alkaline-earth metal water cluster ions.

3. Theories

Since the early 1990's, *ab initio* calculational methods have been applied actively to the study of medium-sized protonated water clusters. Hartree-Fock (HF), density functional theory (DFT), and second-order Møller-Plesset theory (MP2) are three commonly used methods in the electronic energy (EE) calculations. For $H^+(H_2O)_n$ with $n \geq 5$, the MP2 method is probably the highest level of theory that is applicable and it has been shown that MP2 with a large basis set (such as aug-cc-pvDZ [77]) allows accurate characterization of smaller clusters [78–80]. However, due to the unfavorable scaling, MP2/aug-cc-pvDZ is currently restricted to $n \leq 8$ and in practice $H^+(H_2O)_8$ is the largest-sized cluster that permits frequency calculation with MP2/aug-cc-pvDZ on a high-end workstation. The HF method has not gained much popularity in studying $H^+(H_2O)_n$ because of its tendency to overestimate the O–O distance and underestimate the binding energies even for the water dimer. On the other hand, DFT methods (in particular B3LYP) are widely used due to its efficiency and its agreement with experiment. So far, the B3LYP method with a large basis set (aug-cc-pvDZ) has been applied to clusters up to $n = 28$ [40]. We do not give an elaborate comparison here on the performance of different first-principle methods, as extensive discussions of this comparison can be found in [81].

The quest to find the global minimal structure of $H^+(H_2O)_n$ is hindered by the rough energy landscape inherent in the hydrogen-bonded clusters. The existence of large potential energy barriers separating the local minima provokes the quasi-ergodic behavior in simulations. To overcome this sampling problem, Singer *et al.* [82] carried out simulations to study on the structural changes of $H^+(H_2O)_8$ and $H^+(H_2O)_{16}$. Subsequent extensive *ab initio* calculations were carried out to study the isomers recovered from the MC simulations. Similar approaches have been adopted by Christie and Jordan [83] ($n = 6$ and 8), and Kuo and Klein [84] ($n = 5$–22). Hodges and Wales [85] took a different approach and focused on exploring the potential energy landscape using a basin-hopping technique. They gathered a database of low-lying minima for clusters with size up to $n = 21$. Kuo and Klein [84] also searched for the low-lying minima but with a different empirical model. By comparing the results of Hodges and Wales (with the ASP [86] and KJ [87] models) and Kuo and Klein (with the OSS2 [78] model), it is evident that although the general trend for structural changes (tree → single-ring → multiple-ring → cage) with increasing size is similar in both works, the transition sizes and detailed features clearly differ (cf. figure 9). This is a reminder that all these simulations are limited by the accuracy of the empirical models employed, but the recovered inherent structures can be used as a good starting point for further detailed calibrations with high-level *ab initio* calculations. A refined agreement will definitely lead to a better understanding of these interesting ionic clusters and the associated hydrogen bonding in general.

3.1. *Global minimum structures*

The size of the clusters that have been thoroughly studied by *ab initio* methods is presently restricted to $n \leq 8$ (with the exception of $H^+(H_2O)_{21}$) and obviously this is due to the exponentially increasing computational resources involved. On top of that, there

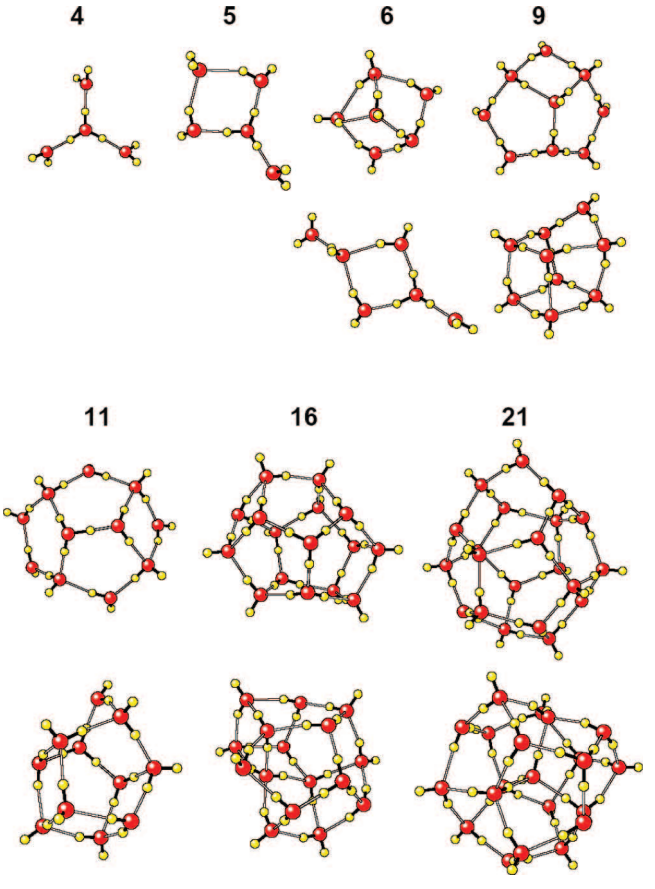

Figure 9. Selected global minima structures of $H^+(H_2O)_n$ under the ASP and OSS2 models. Full lists can be found in figure 1 of [85] and figure 2 of [84]. Although the general trends for structural changes (tree → single-ring → multiple-ring → cage) with increasing size is similar in both works, the transition sizes and detailed features clearly differ.

are several technical issues associated with the *ab initio* calculations such as base set superposition errors (BSSE), zero point energies (ZPE) and ZPE beyond the harmonic oscillator (HO) approximation. In the following, a few examples are used to demonstrate the effects for the above mentioned concerns.

$H^+(H_2O)_5$: This cluster has received much attention from the theoretical community [37, 88–91]. Christie and Jordan [90] found that the structures **311** and **131** shown in figure 10a are iso-energetic under MP2/aug-cc-pvDZ. Their conclusion, however, does not agree with experimental data [37, 70], which indicate that the tree-like isomer **311** predominates the spectrum of $H^+(H_2O)_5$ (cf. figure 6a). The effect of vibrational anharmonicity on the energetic order of different $H^+(H_2O)_5$ isomers has been studied by Mella and Clary [89] and Kuo [91]. In the former, diffusion MC methods with the OSS2 models were used but due to the inadequacy of the models, the relative stability between **311** and **131** cannot be obtained reliably. In the latter, the anharmonicity

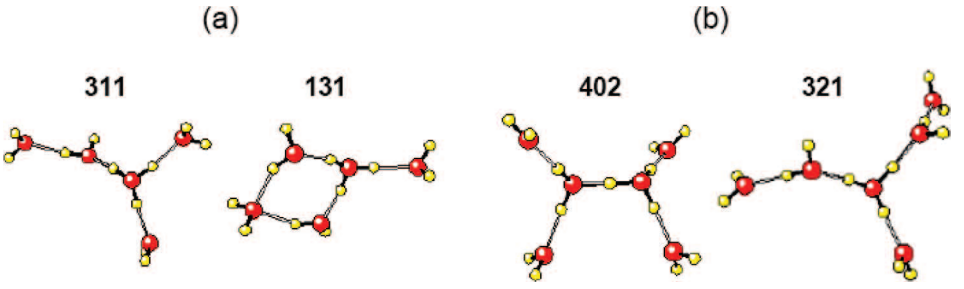

Figure 10. Low-lying minima of (a) $H^+(H_2O)_5$ and (b) $H^+(H_2O)_6$. All the structural isomers are labeled with a three-digit integer, with the first integer being the number of water molecules with single hydrogen bond, the second integer the number of molecules connected with two hydrogen bonds, and so on.

in ZPE was examined by combining the vibrational perturbation theory (VPT2) [92] with *ab initio* methods. After including the anharmonicity correction in ZPE, Kuo [91] found that isomer **311** is indeed more stable than **131** by about 1 mhartree, in accord with the experimental observation (figure 6a).

$H^+(H_2O)_6$: The $H^+(H_2O)_6$ cluster is also one of the most studied cases primarily because it offers the smallest fully solvated Zundel-type structure (**402**) [37, 93–95]. The existence of this isomer (figure 10b) was identified by Jiang *et al.* [37] and their spectra acquired at different temperatures (from ~200 K to as low as 77 K) [39] indicated that the bare $H^+(H_2O)_6$ is composed of a mixture of Zundel-type (**402**) and Eigen-type (**321**) isomers (figures 6b and 10b). Very recently, similar vibrational predissociation experiments by Headrick *et al.* [70] on Ar-attached $H^+(H_2O)_6$ showed strong evidence for the exclusive dominance of the **402** structure. The discrepancy between experiments on bare and Ar-attached species raises concerns on the influence of the attached Ar atom. The role of the Ar attachment on the relative stability of different conformational isomers was investigated by high-level *ab initio* calculations and VPT2 [91], and it is predicted that the Ar-attached **402** is more stable than the Ar-attached **321** by about 1.4 mhartree after inclusion of the vibrational anharmonicity. In the same work, it is concluded that vibrational anharmonicity plays a critical role in determining the energetic ordering among different conformational isomers of $H^+(H_2O)_6$ in a way very similar to $H^+(H_2O)_5$ [91].

$H^+(H_2O)_7$: This cluster has not been the subject of extensive *ab initio* calculations. The only elaborate search was done by Jiang *et al.* [37] and they examined some 14 selected conformational isomers with different topologies covering structures containing an ion core in both Eigen and Zundel types. By comparing the calculated spectra (with B3LYP/6-31 + G*) with the experimental spectra, Jiang *et al.* identified vibrational signatures (between 3500 and 3600 cm^{-1}) belonging to the five-membered ring structures. The identification was verified very recently by Duncan, Johnson, Jordan and coworkers [70] for $H^+(H_2O)_7$-Ar. Thus, $H^+(H_2O)_7$ is likely to be the smallest protonated water cluster with a ring structure as the lowest energy isomer. More thorough searching and higher-level *ab initio* calculations, however, are required to hunt for the global minimum structure of $H^+(H_2O)_7$. An example of these calculations with the vibrational anharmonicity taken into account in ZPE is shown in figure 11 [91].

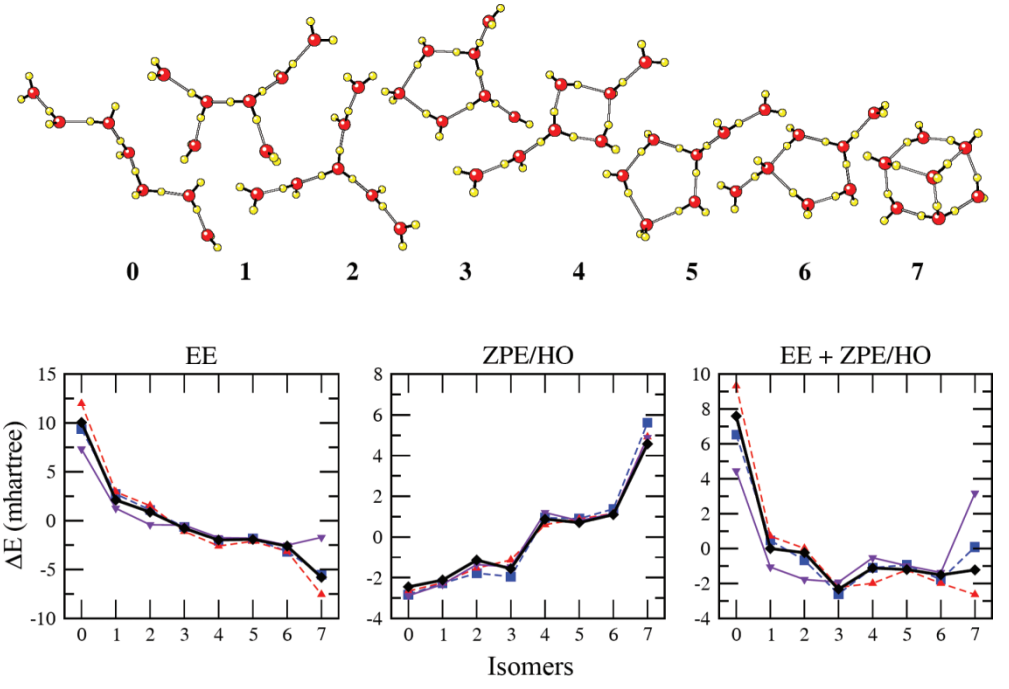

Figure 11. Energy trends on EE, ZPE/HO and EE+ZPE/HO among isomers of $H^+(H_2O)_7$ by several first principle methods: MP2/aug-cc-pvDZ (black diamond), B3LYP/6-31+G* (blue square), MP2/6-31+G* (red triangle up), and B3LYP/aug-cc-pvDZ (purple triangle down). Designations along the *x*-axis refer to the structure shown above. The zero of EE and ZPE/HO scales are the averaged energy of all the isomers listed. It is clear from the figures that compact structures in general have lower electronic energies, and the ZPE under harmonic approximations counteracts this trend. As a result, the energetic ordering is full of many low-lying isomers with very close energies.

$H^+(H_2O)_{8–11}$: Low-lying minima of $H^+(H_2O)_8$ have been studied by Jiang *et al.* [37] and Ciobanu *et al.* [96]. In the former work, the authors only examined a limited number of conformations and in the latter, the authors have conducted a more thorough search on the low-lying minima using an empirical force field and these searched structures were then re-optimized by *ab initio* methods. The same methodology was also used to study the low-lying minima of $H^+(H_2O)_{9–11}$ by Lin *et al.* [41]. It was found that compact structures in general have lower EE than the open ones, but the ZPE under harmonic approximations counteracts this trend. As a result, the energetic ordering is complicated by the existence of many low-lying isomers with very close energies. In light of the errors involved in the DFT methods and the ignorance of the vibrational anharmonicity effect, the prediction of the most stable isomers for these clusters remains a challenge.

$H^+(H_2O)_{12–28}$: Less *ab initio* calculations have been carried out for $n \geq 12$ clusters with the exception of the magic number cluster at $n = 21$. The complexity of the potential energy surface near $n = 20$ makes it very difficult even for empirical models to explore, and the unfavorable scaling of the *ab initio* methods further hinders a thorough first-principle examination. So far, most of the first-principle calculations were done

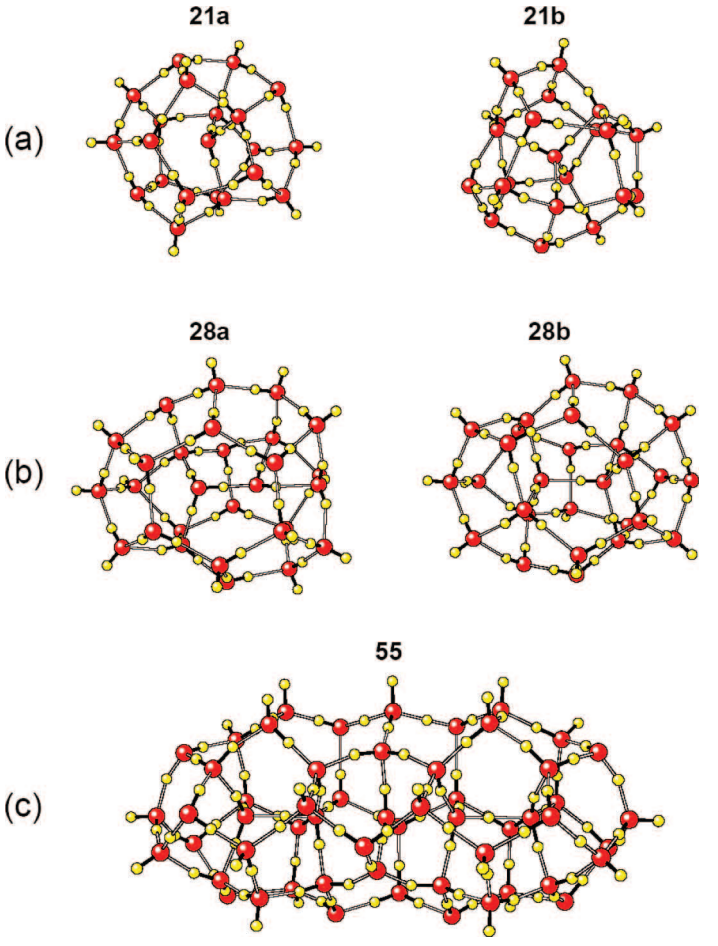

Figure 12. Plausible structures of "magic number" clusters, (a) $H^+(H_2O)_{21}$, (b) $H^+(H_2O)_{28}$, and (c) $H^+(H_2O)_{55}$. The polyhedral cages of each cluster is composed of a mixture of pentagonal and hexagonal rings, denoted as 5^{12} (or 5^65^6) for the 21-mer, $5^{12}6^3$ (or $5^66^35^6$) for the 28-mer, and $5^{12}6^{15}$ (or $5^66^66^36^65^6$) for the 55-mer. The cages of the isomers **21a**, **21b**, **28a**, and **28b** are enclosed with an H_3O^+, an H_2O, an H_3O^+–H_2O and an H_2O-H_2O, respectively [40].

by either HF [97] or DFT [40, 43]. Even though the current theoretical calculations do not reveal a conclusive picture on the global minima structure of $H^+(H_2O)_{21}$, both experimental spectra and theoretical calculations have agreed on the conclusion that cage structures are more stable than open ones. While we could not derive any detailed information regarding the location of the excess proton from the experimental data [40, 43], all *ab initio* calculations indicate the preference for the excess proton (either Eigen or Zundel) to stay on the surface of the cage with the structure shown in figure 12a. Most plausibly, the isomer observed experimentally consists of a clathrate-like cage enclosed with a neutral molecule (**21b**), instead of a hydronium ion (**21a**). The difference in energy between these two isomers is typically more than 5 kcal mol^{-1}, according to the B3LYP/aug-cc-pvDZ//6-31 + G* level of computation. It is worth

mentioning that in $H^+(H_2O)_{28}$, yet again a magic number cluster, the same conclusions regarding the formation of the polyhedral cage and the location of the excess proton can be drawn from the vibrational predissociation spectra and by comparing the relative stabilities of the interior and exterior solvation structures [40]. Figure 12b provides an example for these two types of structure, with either a protonated water dimer (**28a**) or two neutral water molecules (**28b**) encapsulated in the cage.

$H^+(H_2O)_{55}$: A computational venture was launched by our group for $H^+(H_2O)_{55}$, which is a prominent magic number water cluster first identified by Schindler *et al.* [25] and later confirmed by Lee *et al.* [33] with Fourier-transform ICR mass spectrometry. The computation was conducted using the HF method with the 6-31 + G* basis set following the same line of consideration for smaller magic number clusters, $H^+(H_2O)_{21}$ and $H^+(H_2O)_{28}$. Not surprisingly, because of an enormously large number of stable isomers existing for $H^+(H_2O)_{55}$, a thorough search for the low-lying minima is impractical. Shown in figure 12c is one of the low-energy minima on the potential energy surface, which has an intriguing tube-like topology. The surface of the tube-like structure is composed of a mixture of pentagonal and hexagonal rings, and five water molecules are encapsulated within the water nano-tube. Compared to the disc-like structure with a five-fold symmetry as proposed by Niedner-Schatteburg and coworkers [98], this tube-like structure is energetically more stable by $\sim$20 kcal mol^{-1} [99] because more hydrogen bonds are formed between the water molecules. Obviously, assignment of the structure is still in its infancy and further studies (both spectroscopic and computational) are needed to provide more information for this large-sized magic number water cluster.

3.2. *Thermal and dynamical effects*

Monte Carlo (MC) and molecular dynamics methods have been widely used in studying the temperature and dynamical effects on the structure of protonated water clusters. Compared to MC methods, the direct molecular dynamics method is limited by its sampling efficiency, and thus not many molecular dynamics simulations with empirical models have been carried out [100, 101]. It is now possible to carry out *ab initio* molecular dynamics (AIMD) simulations [93, 102–104] in order to eliminate the uncertainty associated with empirical models. However, these AIMD simulations suffer from the same (or worse) limit in sampling efficiency as their classical counterparts. Various MC algorithms, on the other hand, are very efficient in exploring the rough energy landscape intrinsic to the hydrogen-bonded clusters, but so far all the works done along this line are coupled with some empirical models [82–85, 105–108].

A number of empirical models parameterized for $H^+(H_2O)_n$ have been proposed [78, 86, 87, 109, 110], along with many other dissociable water potentials [111–114]. While the increasing computational resource that enables *ab initio* calculations on larger clusters makes the application of analytical empirical models to $H^+(H_2O)_n$ seem obsolete, these models are indispensable for its potential use in acid–base chemistry as well as in large biomolecular systems. In fact, protonated and other ionic water clusters provide an ideal testing ground for further improvement of these analytical models, because high-level *ab initio* calculations and detailed experimental characterizations are becoming available for calibration.

The structural changes of $H^+(H_2O)_n$ with temperature have been carefully examined by a number of research groups [82–84]. Singer *et al*. [82] employed a jump walk (J-walk) algorithm in conjunction with the OSS2 model and found the structures of both $H^+(H_2O)_8$ and $H^+(H_2O)_{16}$ clusters are rather dynamic at temperatures relevant to stratospheric conditions (i.e., ~170 K). However, due to the short simulation length, they could not precisely identify the transition temperature. Christie and Jordan [83] studied smaller clusters (i.e., $H^+(H_2O)_6$ and $H^+(H_2O)_8$) and with a combination of the MS-EVB (multistate empirical valence bond) model and a parallel tempering (PT) algorithm, they found the PT algorithm is an effective means to overcome the quasi-ergodicity.

It is possible to carry out AIMD for larger water clusters and so far most of the simulations of this kind were restricted to the magic number cluster $n = 21$. Due to the computational cost, however, AIMD simulations on protonated water clusters are often restricted by the short simulation length. Nevertheless, Laasonen and Klein [102] found the dodecahedral cages are not stable above 200 K and they also noted that the excess proton seems to prefer to migrate to the surface of the cage. The latter observation is in line with the *ab initio* calculations on the inherent structures mentioned above. With the aim to study the dynamical behavior of the excess proton, more detailed study has been carried out very recently by Iyengar *et al*. [103]. They reconfirmed Laasonen and Klein's findings and additionally found that dynamical effects play an important role in determining the vibrational properties of such clusters.

The temporal dependence of the structure can be thoroughly studied by empirical models with MC techniques. For example, based on the KJ model and the plain Metropolis algorithm, Svanberg and Pettersson [105] focused on the study of solid–liquid transition and noted that the dodecahedral cage of $H^+(H_2O)_{21}$ may melt at ~160 K. To understand these thermal properties, MC simulations in grand canonical ensemble have also been examined by Shevkunov and Vegiri [108] and by Kusaka and Oxtoby [107]. These papers focused on the calculation of thermochemical data and thus provided less structural information about the clusters.

Using the same MC algorithm and the OSS2 model, Kuo and Klein [84] engaged in a systematic study for clusters with size of $n = 5$–22 within the temperature range of 25–330 K. The results of these calculations are exemplified in figure 13 for $H^+(H_2O)_6$ and $H^+(H_2O)_9$ and in figure 14 for $H^+(H_2O)_{18}$. The general trends found by the authors are: (1) tree-like structures dominate at high temperatures for all clusters and single-ring structures appear in slightly lower temperatures at $n \geq 7$, (2) a structural transition (single-ring to multiple-ring) appears upon cooling of the clusters to 100 K at $n \geq 7$, and (3) only at $n \geq 16$ do polyhedral cage structures dominate in the lowest temperature range.

It should be mentioned that the validity of these empirical models is subject to further confirmation with high-level *ab initio* calculations. For example, in studying the location of the excess proton in $H^+(H_2O)_{21}$, molecular dynamics simulations with simple non-polarizable models indicated a preference of the interior solvation of the hydronium ion [100, 115]. However, theoretical simulations with polarizable models and *ab inito* methods all yields results with the opposite trend, that is, the hydronium prefers to reside on the cluster surface [40, 70, 84, 97, 116]. The latter finding is in line with the recent emerging evidences that the polarizability plays a key role in

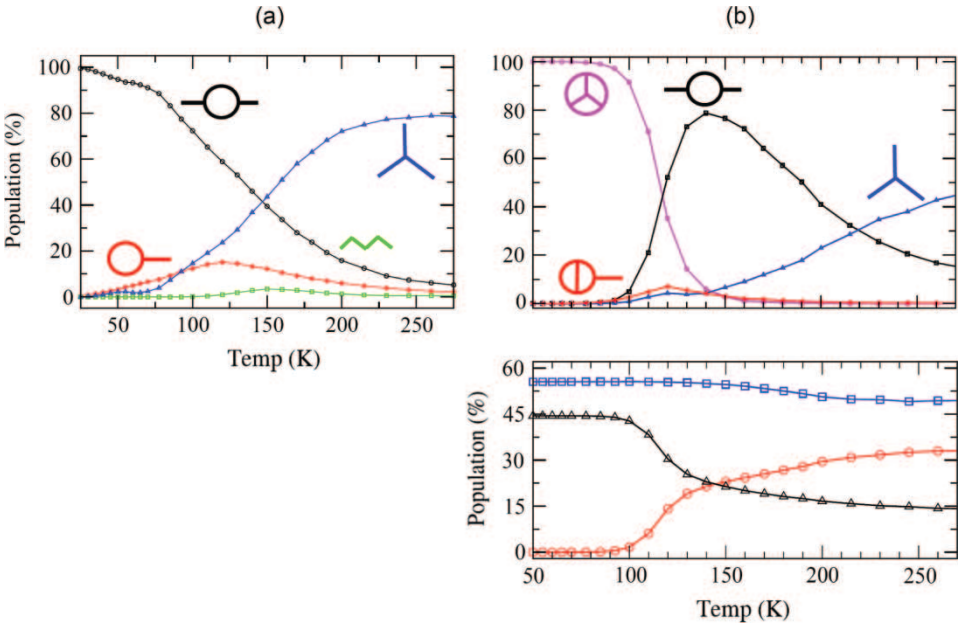

Figure 13. Thermal behaviors of (a) $H^+(H_2O)_6$, and (b) $H^+(H_2O)_9$ from Monte Carlo simulations with the OSS2 potential. The behaviors are shown with population percentages of conformational isomers belonging to different topologies as a function of cluster temperature. The topologies are illustrated with reduced color-coded graphics. Lower panel in (b): percentages of water molecules with different coordination numbers, 1 (red circle), 2 (blue square), and 3 (black triangle) [84].

determining the surface solvation characteristic of the ions [117, 118]. In a sense, the debates over the structures of the protonated water clusters and the effort to obtain a refined agreement between various theories will lead to a better understanding of the many-body interactions between water molecules and between water molecules and the hydrated ions.

4. Conclusion

Elucidating the structure of medium-sized protonated water clusters has taken an integrated approach recently. The approach involves the use of tandem mass spectrometry, vibrational predissociation spectroscopy, high-level *ab initio* calculations, Monte Carlo (MC) and molecular dynamics simulations, as well as a combination of these methods. It has allowed identification of several outstanding features about the structures and thermal properties of $H^+(H_2O)_n$, including formation of symmetric hydrogen bonds at $n = 6$, prevailing of five-membered rings at $n = 7$, and predominance of clathrate-like structures at $n = 21$. These features are distinctly different from those of neutral water molecules, clearly demonstrating the profound influence of the excess proton on the structure of these charged water clusters. While much progress has been made in the past and also recently for $H^+(H_2O)_{5–30}$, many interesting phenomena

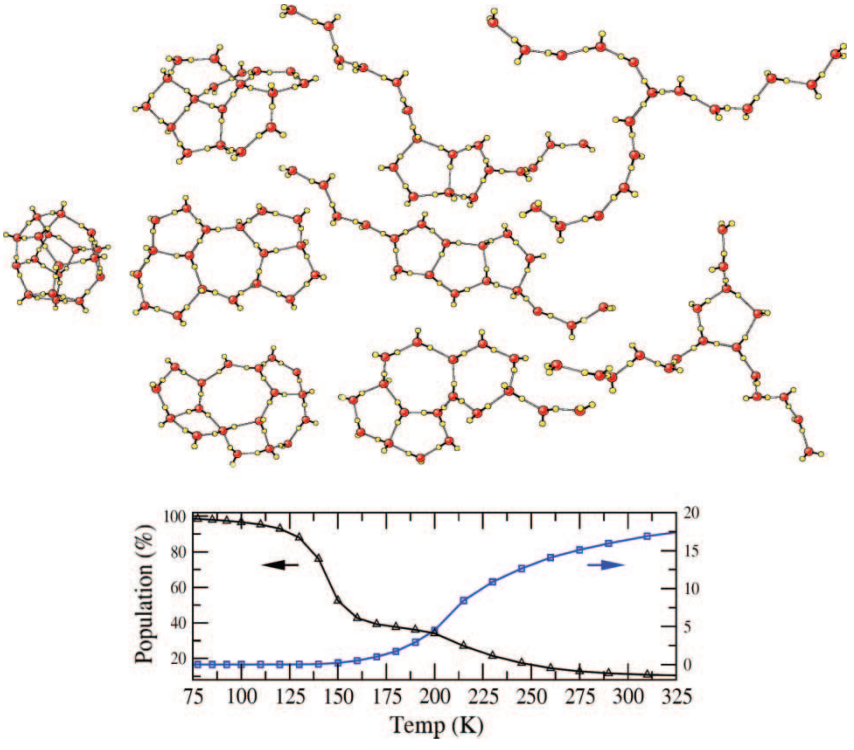

Figure 14. Thermal behaviors of $H^+(H_2O)_{18}$ from Monte Carlo simulations with the OSS2 potential. The graphical analysis is too complicated and not very informative, thus only some representative isomers in each temperature ranges are shown: cage (below 150 K), flowers (150–200 K), and trees (200 K and above). Lower panel: percentages of water molecules with different coordination numbers, 1 (blue square) and 3 (black triangle), as a function of cluster temperature [84].

remain to be observed and controversies to be solved. With the continued development of both experimental and theoretical techniques, it is expected that our understanding of these fundamentally important but yet complex cluster systems can be further improved in the near future.

Acknowledgements

This research is supported by grants from Academia Sinica and the National Science Council (Grant No. NSC 93-2113-M-001-045) of Taiwan. The authors thank G. Niedner-Schatteburg for providing his suggested structure and J. C. Jiang for calculating the structures of the $n = 55$ cluster.

References

[1] K. Liu, J. D. Cruzan, and R. J. Saykally, Sci. **271,** 929 (1996).
[2] F. N. Keutsch and R. J. Saykally, Proc. Natl. Acad. Sci. USA **98,** 10533 (2001).
[3] F. N. Keutsch, J. D. Cruzan, and R. J. Saykally, Chem. Rev. **103,** 2533 (2003).

[4] U. Buck and F. Huisken, Chem. Rev. **100,** 3863 (2000).
[5] V. Buch, S. Bauerecker, J. P. Devlin, U. Buck, and J. K. Kazimirski, Int. Rev. Phys. Chem. **23,** 375 (2004).
[6] E. E. Ferguson and F. Arnold, Acc. Chem. Res. **14,** 327 (1981).
[7] R. P. Wayne, *Chemistry of Atmospheres* (Oxford University Press, Oxford, 1991).
[8] J. H. Seinfeld and S. N. Pandis, *Atmospheric Chemistry and Physics: From Air Pollution to Climate Change* (Wiley, New York, 1998).
[9] M. Okumura, L. I. Yeh, J. D. Myers, and Y. T. Lee, J. Chem. Phys. **85,** 2328 (1986).
[10] L. I. Yeh, M. Okumura, J. D. Myers, J. M. Price, and Y. T. Lee, J. Chem. Phys. **91,** 7319 (1989).
[11] L. I. Yeh, Y. T. Lee, and J. T. Hougen, J. Mol. Spectrosc. **164,** 473 (1994).
[12] K. R. Asmis, N. L. Pivonka, G. Santambrogio, M. Brümmer, C. Kaposta, D. M. Neumark, and L. Wöste, Sci. **299,** 1375 (2003).
[13] T. D. Fridgen, T. B. McMahon, L. MacAleese, J. Lemaire, and P. Maitre, J. Phys. Chem. A **108,** 9008 (2004).
[14] T. D. Fridgen, L. MacAleese, P. Maitre, T. B. McMahon, P. Boissel, and J. Lemaire, Phys. Chem. Chem. Phys. **7,** 2747 (2005).
[15] E. Kochanski, R. Kelterbaum, S. Klein, M. M. Rohmer, and A. Rahmouni, Adv. Quantum Chem. **28,** 273 (1997).
[16] X. C. Huang, H. M. Cho, S. Carter, L. Ojamae, J. M. Bowman, and S. J. Singer, J. Phys. Chem. A **107,** 7142 (2003).
[17] A. B. McCoy, X. C. Huang, S. Carter, M. Y. Landeweer, and J. M. Bowman, J. Chem. Phys. **122,** 061101 (2005).
[18] X. C. Huang, B. J. Braams, and J. M. Bowman, J. Chem. Phys. **122,** 044308 (2005).
[19] G. Niedner-Schatteburg and V. E. Bondybey, Chem. Rev. **100,** 4059 (2000).
[20] P. Kebarle, S. K. Searles, A. Zolla, J. Scarborough, and M. Arshadi, J. Am. Chem. Soc. **89,** 6393 (1967).
[21] A. J. Cunningham, J. D. Payzant, and P. Kebarle, J. Am. Chem. Soc. **94,** 7627 (1972).
[22] P. Kebarle, Annu. Rev. Phys. Chem. **28,** 445 (1977).
[23] A. J. Stace and C. Moore, Chem. Phys. Lett. **96,** 80 (1983).
[24] O. Echt, D. Kreisle, M. Knapp, and E. Recknagel, Chem. Phys. Lett. **108,** 401 (1984).
[25] T. Schindler, C. Berg, G. Niedner-Schatteburg, and V. E. Bondybey, Chem. Phys. Lett. **250,** 301 (1996).
[26] K. Honma, L. S. Sunderlin, and P. B. Armentrout, J. Chem. Phys. **99,** 1623 (1993).
[27] Y. Kawai, S. Yamaguchi, Y. Okada, and K. Takeuchi, Int. J. Mass Spectrom. **220,** 375 (2002).
[28] S. Yamaguchi, S. Kudoh, Y. Okada, T. Orii, K. Takeuchi, T. Ichikawa, and H. Nakai, J. Phys. Chem. A **107,** 10904 (2003).
[29] C. M. Nelson and M. Okumura, J. Phys. Chem. **96,** 6112 (1992).
[30] T. Schindler, C. Berg, G. Niedner-Schatteburg, and V. E. Bondybey, J. Chem. Phys. **104,** 3998 (1996).
[31] U. Achatz, S. Joos, C. Berg, T. Schindler, M. Beyer, G. Albert, G. Niedner-Schatteburg, and V. E. Bondybey, J. Am. Chem. Soc. **120,** 1876 (1998).
[32] S. E. Rodriguez-Cruz, J. S. Klassen, and E. R. Williams, J. Am. Soc. Mass Spectrom. **8,** 565 (1997).
[33] S. W. Lee, P. Freivogel, T. Schindler, and J. L. Beauchamp, J. Am. Chem. Soc. **120,** 11758 (1998).
[34] M. W. Crofton, J. M. Price, and Y. T. Lee, 1994, In *Clusters of Atoms and Molecules*, H. Haberland, Ed., Springer-Verlag, Berlin, 45.
[35] Y.-S. Wang, J. C. Jiang, C.-L. Cheng, S. H. Lin, Y. T. Lee, and H.-C. Chang, J. Chem. Phys. **107,** 9695 (1997).
[36] H.-C. Chang, J. C. Jiang, H.-C. Chang, Y.-S. Wang, S. H. Lin, and Y. T. Lee, J. Chin. Chem. Soc. **46,** 427 (1999).
[37] J. C. Jiang, Y.-S. Wang, H.-C. Chang, S. H. Lin, Y. T. Lee, G. Niedner-Schatteburg, and H.-C. Chang, J. Am. Chem. Soc. **122,** 1398 (2000).
[38] C.-C. Wu, C. Chaudhuri, J. C. Jiang, Y. T. Lee, and H.-C. Chang, J. Chin. Chem. Soc. **49,** 769 (2002).
[39] Y.-S. Wang, C.-H. Tsai, Y. T. Lee, H.-C. Chang, J. C. Jiang, O. Asvany, S. Schlemmer, and D. Gerlich, J. Phys. Chem. A **107,** 4217 (2003).
[40] C.-C. Wu, C.-K. Lin, H.-C. Chang, J. C. Jiang, J.-L. Kuo, and M. L. Klein, J. Chem. Phys. **122,** 074315 (2005).
[41] C.-K. Lin, C.-C. Wu, Y.-S. Wang, Y. T. Lee, H.-C. Chang, J.-L. Kuo, and M. L. Klein, Phys. Chem. Chem. Phys. **7,** 938 (2005).
[42] M. Miyazaki, A. Fujii, T. Ebata, and N. Mikami, Sci. **304,** 1134 (2004).
[43] J.-W. Shin, N. I. Hammer, E. G. Diken, M. A. Johnson, R. S. Walters, T. D. Jaeger, M. A. Duncan, R. A. Christie, and K. D. Jordan, Sci. **304,** 1137 (2004).
[44] M. Meot-Ner and C. V. Speller, J. Phys. Chem. **90,** 6616 (1986).
[45] D. A. Wild and E. J. Bieske, Int. Rev. Phys. Chem. **22,** 129 (2003).
[46] O. Dopfer, Int. Rev. Phys. Chem. **22,** 437 (2003).
[47] J. M. Farrar, Int. Rev. Phys. Chem. **22,** 593 (2003).

[48] Y.-S. Wang, H.-C. Chang, J. C. Jiang, S. H. Lin, Y. T. Lee, and H.-C. Chang, J. Am. Chem. Soc. **120,** 8777 (1998).
[49] B. Rowland and J. P. Devlin, J. Chem. Phys. **94,** 812 (1991).
[50] V. Buch and J. P. Devlin, J. Chem. Phys. **94,** 4091 (1991).
[51] J. C. Jiang, J.-C. Chang, B.-C. Wang, S. H. Lin, Y. T. Lee, and H.-C. Chang, Chem. Phys. Lett. **289,** 373 (1998).
[52] S. S. Lin, Rev. Sci. Instrum. **44,** 516 (1973).
[53] J. Q. Searcy and J. B. Fenn, J. Chem. Phys. **61,** 5282 (1974).
[54] R. I. Beuhler and L. Friedman, J. Chem. Phys. **77,** 254 (1982).
[55] V. Hermann, B. D. Kay, and A. W. Castleman Jr, Chem. Phys. **72,** 185 (1982).
[56] X. Yang and A. W. Castleman Jr, J. Am. Chem. Soc. **111,** 6845 (1989).
[57] X. Yang, X. Zhang, and A. W. Castleman Jr, Int. J. Mass Spectrom. Ion Processes **109,** 339 (1991).
[58] S. Wei, Z. Shi, and A. W. Castleman Jr, J. Chem. Phys. **94,** 3268 (1991).
[59] Z. Shi, J. V. Ford, S. Wei, and A. W. Castleman Jr, J. Chem. Phys. **99,** 8009 (1993).
[60] X. Zhang and A. W. Castleman Jr, J. Chem. Phys. **101,** 1157 (1994).
[61] E. D. Sloan, Nature **426,** 353 (2003).
[62] H. Shinohara, U. Nagashima, and N. Nishi, Chem. Phys. Lett. **111,** 511 (1984).
[63] U. Nagashima, H. Shinohara, N. Nishi, and H. Tanaka, J. Chem. Phys. **84,** 209 (1986).
[64] M. Eigen and L. D. Maeyer, Proc. R. Soc. London **A247,** 505 (1958).
[65] M. Eigen, Angew. Chem. **3,** 1 (1964).
[66] G. Zundel, In *The Hydrogen Bond: Recent Developments in Theory and Experiment*, edited by P. Schuster, G. Zundel and C. Sandory (North-Holland, Amsterdam, 1976), Vol. 2, Chapter 15.
[67] W. Danninger and G. Zundel, J. Chem. Phys. **74,** 2769 (1981).
[68] J. M. Headrick, J. C. Bopp, and M. A. Johnson, J. Chem. Phys. **121,** 11523 (2004).
[69] N. I. Hammer, E. G. Diken, J. R. Roscioli, M. A. Johnson, E. M. Myshakin, K. D. Jordan, A. B. McCoy, X. Huang, J. M. Bowman, and S. Carter, J. Chem. Phys. **122,** 244301 (2005).
[70] J. M. Headrick, E. G. Diken, R. S. Walters, N. I. Hammer, R. A. Christie, J. Cui, E. M. Myshakin, M. A. Duncan, M. A. Johnson, and K. D. Jordan, Sci. **308,** 1765 (2005).
[71] H.-C. Chang, J. C. Jiang, S. H. Lin, Y. T. Lee, and H.-C. Chang, J. Phys. Chem. A **103,** 2941 (1999).
[72] H.-C. Chang, J. C. Jiang, H.-C. Chang, L. R. Wang, and Y. T. Lee, Isr. J. Chem. **39,** 231 (2000).
[73] N. Solca and O. Dopfer, J. Am. Chem. Soc. **126,** 9520 (2004).
[74] N. Solca and O. Dopfer, J. Phys. Chem. A **109,** 6174 (2005).
[75] E. R. Lovejoy and R. Bianco, J. Phys. Chem. A **104,** 10280 (2000).
[76] R. L. Wong, K. Paech, and E. R. Williams, Int. J. Mass Spectrom. **232,** 59 (2004).
[77] J. T. H. Dunning, J. Chem. Phys. **90,** 1007 (1989).
[78] L. Ojamae, I. Shavitt, and S. J. Singer, Int. J. Quantum Chem. **Suppl. 29,** 657 (1995).
[79] J. E. del Bene, M. J. Frisch, and J. A. Pople, J. Phys. Chem. **89,** 3669 (1985).
[80] L. Ojamae, I. Shavitt, and S. J. Singer, J. Chem. Phys. **109,** 5547 (1998).
[81] W. Koch and M. C. Holthausen, *A Chemist's Guide to Density Functional Theory*, 2nd ed. (Wiley, Weinheim, 2001).
[82] S. J. Singer, S. McDonald, and L. Ojamae, J. Chem. Phys. **112,** 710 (2000).
[83] R. A. Christie and K. D. Jordan, J. Phys. Chem. B **106,** 8376 (2002).
[84] J.-L. Kuo and M. L. Klein, J. Chem. Phys. **122,** 024516 (2005).
[85] M. P. Hodges and D. J. Wales, Chem. Phys. Lett. **324,** 279 (2000).
[86] M. P. Hodges and A. J. Stone, J. Chem. Phys. **110,** 6766 (1999).
[87] R. E. Kozack and P. C. Jordan, J. Chem. Phys. **96,** 3131 (1992).
[88] G. Corongiu, R. Kelterbaum, and E. Kochanski, J. Phys. Chem. **99,** 8038 (1995).
[89] M. Mella and D. C. Clary, J. Chem. Phys. **119,** 10048 (2003).
[90] R. A. Christie and K. D. Jordan, J. Phys. Chem. A **105,** 7551 (2001).
[91] J.-L. Kuo, J. Phys. Conf. Ser. (in press).
[92] V. Barone, J. Chem. Phys. **122,** 014108 (2005).
[93] H. P. Cheng, J. Phys. Chem. A **102,** 6201 (1998).
[94] D. Wei and D. R. Salahub, J. Chem. Phys. **106,** 6086 (1997).
[95] M. Mella, J.-L. Kuo, D. C. Clary, and M. L. Klein, Phys. Chem. Chem. Phys. **7,** 2324 (2005).
[96] C. V. Ciobanu, L. Ojamae, I. Shavitt, and S. J. Singer, J. Chem. Phys. **113,** 5321 (2000).
[97] A. Khan, Chem. Phys. Lett. **319,** 440 (2000).
[98] V. E. Bondybey, T. Schindler, C. Berg, M. Beyer, U. Achatz, S. Joos, and G. Niedner-Schatteburg, In *Recent Theoretical and Experimental Advances in Hydrogen Bonded Clusters*, edited by S. S. Xantheas (Kluwer Academic, Dordrecht, 2000), NATO ASI Ser., Ser. C, Vol. 561, 323.
[99] J. C. Jiang, C.-K. Lin, C.-C. Wu, and H.-C. Chang, unpublished results.
[100] E. Brodskaya, A. P. Lyubartsev, and A. Laaksonen, J. Chem. Phys. **116,** 7879 (2002).
[101] A. V. Egorov, E. N. Brodskaya, and A. Laaksonen, J. Chem. Phys. **118,** 6380 (2003).

[102] K. Laasonen and M. L. Klein, J. Phys. Chem. **98,** 10079 (1994).
[103] S. S. Iyengar, M. K. Peterson, T. J. F. Day, C. J. Burnham, V. E. Teige, and G. A. Voth, J. Chem. Phys. **123,** 084309 (2005).
[104] S. S. Iyengar, T. J. F. Day, and G. A. Voth, Int. J. Mass. Spectrom. **241,** 197 (2005).
[105] M. Svanberg and J. B. C. Pettersson, J. Phys. Chem. A **102,** 1865 (1998).
[106] T. James and D. J. Wales, J. Chem. Phys. **122,** 134306 (2005).
[107] I. Kusaka and D. W. Oxtoby, J. Chem. Phys. **113,** 10100 (2000).
[108] S. V. Shevkunov and A. Vegiri, J. Chem. Phys. **111,** 9303 (1999).
[109] U. W. Schmitt and G. A. Voth, J. Phys. Chem. B **102,** 5547 (1998).
[110] S. V. Shevkunov and A. Vegiri, Mol. Phys. **98,** 149 (2000).
[111] F. H. Stillinger and C. W. David, J. Chem. Phys. **69,** 1473 (1978).
[112] J. W. Halley, J. R. Rustad, and A. Rahman, J. Chem. Phys. **98,** 4110 (1993).
[113] N. Kumagai, K. Kawamura, and T. Yokokawa, Mol. Simul. **12,** 177 (1994).
[114] C. W. David, J. Chem. Phys. **104,** 7255 (1996).
[115] E. Brodskaya, A. P. Lyubartsev, and A. Laaksonen, J. Phys. Chem. B **106,** 6479 (2002).
[116] D. J. Wales and M. P. Hodges, Chem. Phys. Lett. **286,** 65 (1998).
[117] E. M. Knipping, M. J. Lakin, K. L. Foster, P. Jungwirth, D. J. Tobias, R. B. Gerber, D. Dabdub, and B. J. Finlayson-Pitts, Sci. **288,** 301 (2000).
[118] P. Jungwirth and D. J. Tobias, J. Phys. Chem. B **106,** 6361 (2002).